CrossMark

J. Fluid Mech. (2018), *vol.* 845, *pp.* 392–416. © Cambridge University Press 2018
doi:10.1017/jfm.2018.260

A mechanism for jet drift over topography

Hemant Khatri[1],† **and Pavel Berloff**[1]

[1]Department of Mathematics, Imperial College London, London SW7 2AZ, UK

(Received 14 October 2017; revised 17 January 2018; accepted 20 March 2018;
first published online 26 April 2018)

The dynamics of multiple alternating oceanic jets has been studied in the presence of a simple bottom topography with constant slope in the zonal direction. A baroclinic quasi-geostrophic model forced with a horizontally uniform and vertically sheared background flow generates mesoscale eddies and jets that are tilted from the zonal direction and drift with constant speed. The governing dynamical equations are rewritten in a tilted frame of reference moving with the jets, and the cross-jet time-mean profiles of the linear and nonlinear stress terms are analysed. Here, the linear stress terms are present because of the zonally asymmetric topography. It is demonstrated that the linear dynamics controls the drift mechanism. Also, it is found that the drifting jets are directly forced by the imposed vertical shear, whereas the eddies oppose the jets, although this is limited to continuously forced dissipative systems. This role of the eddies is opposite to the one in the classical baroclinic model of stationary, zonally symmetric multiple jets. This is expected to be more generic in the ocean, which is zonally asymmetric nearly everywhere.

Key words: baroclinic flows, quasi-geostrophic flows, topographic effects

1. Introduction

Rapidly rotating atmospheres behave like quasi-two-dimensional fluids, in which an upscale transfer of energy results in the formation of large-scale patterns (Charney 1971). For example, zonally banded structures commonly referred to as 'alternating jets' are seen in the atmospheres of Jupiter and Saturn (Beebe *et al.* 1980; Gierasch, Conrath & Magalha 1986; Read *et al.* 2009). In such atmospheres, the upscale transfer of energy (see Young & Read 2017), supplied by baroclinic instabilities and small-scale convection due to internal heating, leads to an alternating jet pattern. Rhines (1975) first proposed a mechanism for jet formation, in which the upscale energy transfer is modified by the presence of Rossby waves (i.e. the 'β-effect' due to Coriolis parameter meridional gradient β) and channelled into zonal structures. The presence of alternating jets has been confirmed in a variety of eddying nonlinear model solutions (Williams 1979; Panetta 1993; Vallis & Maltrud 1993; Cho & Polvani 1996; Huang & Robinson 1998; and others) and it has been observed that the meridional width of the jets is controlled by the magnitude of β and the eddy energy (Rhines 1975; Maltrud & Vallis 1991; Vallis & Maltrud 1993; Scott & Polvani 2007; Sukoriansky, Dikovskaya & Galperin 2007; Chemke & Kaspi 2015*a*).

† Email address for correspondence: h.khatri16@imperial.ac.uk

https://doi.org/10.1017/jfm.2018.260 Published online by Cambridge University Press

More recently, oceanic multiple alternating jets (sometimes referred to as 'latent jets' or 'striations') have been observed in satellite altimetry, float datasets and eddy-resolving ocean general circulation models (Maximenko, Bang & Sasaki 2005; Nakano & Hasumi 2005; Richards *et al.* 2006; Sokolov & Rintoul 2007; Van Sebille, Kamenkovich & Willis 2011; Cravatte, Kessler & Marin 2012; Buckingham & Cornillon 2013; Cravatte *et al.* 2017). There is general agreement that at leading order the oceanic jets can be explained by quasi-geostrophic (QG) dynamics with the β-effect (Kramer *et al.* 2006; Nadiga 2006). However, ambiguities remain about their generation mechanisms, the relative importance of the barotropic and baroclinic modes, and the interactions between the jets and eddies. Jet formation may be predicted by the stochastic structural theory in the β-plane barotropic turbulence (Farrell & Ioannou 2007; Marston, Conover & Schneider 2008; Srinivasan & Young 2012; Constantinou, Farrell & Ioannou 2014). Alternatively, Berloff (2005*b*) and Berloff, Kamenkovich & Pedlosky (2009*a*,*b*) explained the jet formation in terms of interacting multiscale eigenmodes and non-local energy transfers to zonal eigenmodes, and further argued that the width of the jets is controlled by the first baroclinic deformation radius. Furthermore, Berloff & Kamenkovich (2013*a*,*b*) showed that, despite the essential nonlinearity, the jets and eddies are significantly controlled by underlying linear dynamics. It is argued that the jets can be explained by spatially inhomogeneous stirring of potential vorticity (PV) that results in a 'staircase' structure of the meridional PV profile (see figure 5 in McIntyre 1982), where the jets reside at the PV interfaces (Baldwin *et al.* 2007; Dritschel & McIntyre 2008; Dunkerton & Scott 2008). Other factors such as instability of meridional boundary currents (Hristova, Pedlosky & Spall 2008; Wang *et al.* 2012), secondary or modulational instability of Rossby waves (Berloff 2005*b*; Connaughton *et al.* 2010; Qiu, Chen & Sasaki 2013) and bottom topography (Sinha & Richards 1999) can also induce multiple alternating jets.

In this paper, we explore the effects of bottom topography on oceanic baroclinic jets, eddies and their dynamics. In particular, transient braided jets steered by topography have been found in many situations (Sokolov & Rintoul 2007; Thompson 2010; Thompson & Richards 2011; Chen, Kamenkovich & Berloff 2015). The jet transport properties also tend to be significantly different in the presence of topography. For example, with a two-dimensional topography, the meridional eddy-induced transport increases with increasing topographic steepness because of induced non-zonal mean flows (Thompson 2010; see also Tréguier & Panetta 1994). While studying the effects of zonally sloping topography, Boland *et al.* (2012) found that jets drift meridionally and tilt with respect to the zonal direction at an angle that increases with the zonal component of PV gradient. Tilted and drifting jets have also been found in Argo float data and comprehensive ocean circulation models (Nakano & Hasumi 2005; Van Sebille *et al.* 2011; Stern, Nadeau & Holland 2015; Chen, Kamenkovich & Berloff 2016). It has been shown that the jets tilt towards the tilted isolines of the mean barotropic PV (Boland *et al.* 2012). However, there is no clear explanation of why the jets drift. Boland *et al.* (2012) and Chen *et al.* (2016) hypothesise that the drift is controlled by linear dynamics. Thompson & Richards (2011) and Chen *et al.* (2015) studied the dynamics of jets in the presence of meridional ridges. They found that the jets, which are present downstream of the ridge, are pushed in the meridional direction because of offset nonlinear eddy forcing.

In this work, we specifically concentrate on the drifting behaviour of multiple alternating jets in baroclinic eddying flows. Similar to Boland *et al.* (2012), a simple topography is considered that increases linearly in the zonal direction. The effects

https://doi.org/10.1017/jfm.2018.260 Published online by Cambridge University Press

of the resulting zonal asymmetry on the dynamics of alternating jets are studied in a two-layer QG model forced with a horizontally uniform, zonal, vertical shear. Statistically equilibrated nonlinear flow solutions show the presence of meridionally drifting tilted jets, as in Boland *et al.* (2012). The drift velocities are then compared with predictions from the linear dynamics. In the later part, we use a non-stationary, tilted frame of reference to study the nonlinear and linear stress terms in the time-averaged dynamical balances, as well as their correlations with the mean PV. The nonlinear eddy forcing is further decomposed into the Reynolds stress term and form stress term, and their roles in the maintenance of the jets are investigated. Eddy fluxes of relative vorticity and buoyancy are also analysed. The transformation of the governing equations into the non-stationary frame of reference is helpful, because, in the new set of equations, the jet drift speed becomes an explicit parameter, whereas the jets become stationary. This way, the mean flow can be easily separated from transient eddies, thus helping to understand the jet drift mechanism.

The paper is organised into four sections. The model is described in § 2. The next section, § 3, is divided into five parts. In the first two parts, jet drift speeds in the nonlinear flow solutions are compared with the predictions from the linear dispersion relation, and also the nonlinear eddy effects are investigated. In the latter parts, we discuss a physical mechanism for the jet drift, and analyse how the system approaches its equilibrium state. The conclusions are in § 4. The mathematical derivations are given in appendix A.

2. Model details

A two-layer QG model with bottom topography on the β-plane, forced with an upper-layer horizontally uniform, zonal, steady background flow U_b, is used in the study (a sketch of the domain is shown in figure 1). The governing equations in the presence of bottom topography are (Vallis 2017):

$$\frac{\mathrm{D}_1}{\mathrm{D}t}[\nabla^2\psi_1 + S_1(\psi_2 - \psi_1 + U_b y)] + \beta\frac{\partial\psi_1}{\partial x} = \nu\nabla^4\psi_1, \tag{2.1}$$

$$\begin{aligned}\frac{\mathrm{D}_2}{\mathrm{D}t}&[\nabla^2\psi_2 + S_2(\psi_1 - U_b y - \psi_2)] \\ &+ \left(\beta + \frac{f_o}{H_2}\frac{\partial\eta_T}{\partial y}\right)\frac{\partial\psi_2}{\partial x} - \frac{f_o}{H_2}\frac{\partial\eta_T}{\partial x}\frac{\partial\psi_2}{\partial y} = \nu\nabla^4\psi_2 - \gamma\nabla^2\psi_2,\end{aligned} \tag{2.2}$$

where $i = 1, 2$ indicate the top and bottom isopycnal layers, respectively; ψ_i is the layer-wise velocity streamfunction; β is the meridional gradient of the Coriolis parameter $f = f_o + \beta y$ (f_o is the angular velocity due to the Earth's rotation at some reference latitude); H_i is the layer thickness; η_T is the bottom topography; $S_i = f_o^2/g'H_i$ (with $g' = g(\rho_2 - \rho_1)/\rho_1$, g the gravity acceleration and ρ_i the layer density) is the stratification parameter in each layer; and ν, γ are eddy viscosity and bottom friction parameters, respectively. Note that

$$\frac{\mathrm{D}_i}{\mathrm{D}t} = \frac{\partial}{\partial t} - \frac{\partial}{\partial y}(\psi_i - \delta_{i1}U_b y)\frac{\partial}{\partial x} + \frac{\partial}{\partial x}(\psi_i - \delta_{i1}U_b y)\frac{\partial}{\partial y}, \tag{2.3}$$

where $\delta_{ij} = 1$ if $i = j$, else $\delta_{ij} = 0$.

https://doi.org/10.1017/jfm.2018.260 Published online by Cambridge University Press

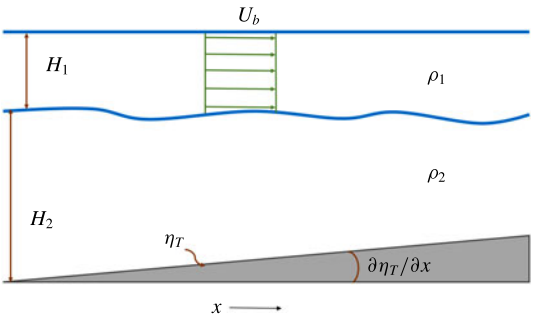


FIGURE 1. (Colour online) Sketch of the model domain. The upper layer has an imposed uniform eastward background flow U_b; H_i and ρ_i are the layer depth and layer density in each layer, respectively; and η_T is the bottom topography. Axis y points into the sketch.

2.1. *Model parameters and spin-up*

The computations were performed on a doubly periodic rectangular domain having uniform spatial resolution of 512×256 grid points, with the domain length L_x kept twice the width L_y ($L_x = 3600$ km; x and y are the zonal and meridional coordinates, respectively). Most of the parameter values are adapted from Berloff *et al.* (2009*b*), i.e. $\beta = 2 \times 10^{-11}$ m^{-1} s^{-1}, $H_1 = 1$ km, $H_2 = 3$ km, $S_1 = 1.2 \times 10^{-9}$ m^{-2} and $S_2 = 0.4 \times 10^{-9}$ m^{-2}. The value of β is at 30° latitude, and the stratification parameters correspond to a baroclinic deformation radius of 25 km, which is typical in the mid-latitudinal ocean (Chelton *et al.* 1998). We chose background flow U_b equal to 0.06 m s^{-1}, which is a baroclinically unstable flow for the chosen parameter values. Values $\nu = 100$ m^2 s^{-1} and $\gamma = 2 \times 10^{-8}$ s^{-1} were used to remove excess energy from the system. The bottom drag coefficient value has been kept quite small, so that the developed jets are strong and clear – the effects of bottom friction are discussed in Berloff *et al.* (2011).

In this work, we analyse the impacts of a slowly varying topography such that $(f_o/H_2)|\nabla\eta_T|$ is smaller than β; hence, the β-effect controls the jet formation. The idea is to understand the effects of bottom topography on jets that are primarily formed by the β-effect, and not to modify the baroclinic instability process. The dynamics over a very steep topography would also be very interesting to study, but we do not address that in this paper. Here, we concentrate only on the effects of the zonal asymmetry, as a meridional gradient in η_T would be equivalent to an additional β-effect in the deep layer (from (2.2)). Given that β controls the jet formation, a small meridional slope is unlikely to change the dynamics significantly. In fact, we ran a test simulation with a small meridional slope, and compared the flow patterns with a flat bottom simulation. The jets were stationary in both cases, and we observed a negligible difference in the flow patterns. In this work, we consider a topography that increases linearly in the zonal direction. We consider three different cases for $T_x = (f_o/H_2)(\partial\eta_T/\partial x)$: 8.3×10^{-13}, 1.4×10^{-12} and 2.8×10^{-12} m^{-1} s^{-1}. Note that T_x is still quite small in comparison to β, and the change in depth is also small compared to the thickness of the lower layer. Here we refer to these as 'small slope', 'medium slope' and 'large slope', respectively.

In the numerical simulations, (2.1) and (2.2) were discretised using a second-order finite-difference method and solved with an advanced numerical scheme called CABARET (Karabasov, Berloff & Goloviznin 2009). The simulations were initialised from a perturbed background state and run for 20 000 days. The system quickly

https://doi.org/10.1017/jfm.2018.260 Published online by Cambridge University Press

develops mesoscale eddies which then transfer energy upscale to form alternating jets. The jets were largely formed by the simulation time of 1000 days, and it took approximately 4000 days more to reach a statistically steady state, with completely matured jets.

3. Results

At first, we study the behaviour of alternating jets in the equilibrium state, in which time-mean energy supplied to the system by the background flow is equal to the energy removed by viscous dissipation and bottom drag. Snapshots of the PV anomaly field in the top layer ($\nabla^2\psi_1 + S_1(\psi_2 - \psi_1)$) and bottom layer ($\nabla^2\psi_2 + S_2(\psi_1 - \psi_2)$) are shown in figure 2(*a–f*). Alternating jets are tilted from the zonal direction, and the angle increases with the bottom slope (tilt angles are 5.71°, 7.13° and 9.46° in the corresponding reference solutions). Here, the direction of the background PV gradient in the bottom layer ($\boldsymbol{\nabla}[f_o + (\beta - S_2U_b)y + T_x x]$) is no longer meridional due to the presence of the zonal asymmetry, and makes a certain angle with the top-layer background PV gradient ($\boldsymbol{\nabla}[f_o + (\beta + S_1U_b)y]$). This affects the direction of Rossby wave propagation and results in the tilted jets. The angle of tilt can be easily estimated in a barotropic model as $\tan^{-1}(T_x/\beta)$ (Boland *et al.* 2012). However, the dynamics is more complex in multilayer models, where the tilt angle is determined by the combined dynamics of both layers. In the two-layer QG model experiments, Boland *et al.* (2012) observed that the jets tend to be aligned with the mean barotropic background PV isolines, but there were deviations. In our simulations, the jet tilt angles are always larger than the ones estimated analytically from the barotropic background PV ($\theta = \tan^{-1}[H_2T_x/((H_1 + H_2)\beta)]$), which are 1.78°, 3.01° and 5.99° for the chosen slopes. Also, the periodic boundary conditions restrict the jets to tilt at specific angles, because in order to satisfy the boundary conditions, the number of jet pairs has to be an integer, and also the jets have to be evenly spaced. Note that the spatial structure of the PV anomaly field is quite different in the bottom layer in comparison to the top layer. As mentioned above, the mean PV isolines in the layers are no longer parallel; on the other hand, the jets are parallel in both layers. As a result of this, the jets actually cross the mean PV isolines in the bottom layer, which leads to the differences in the PV spatial structure.

In addition to tilting, the jets drift in the direction perpendicular to their phase lines (see Hovmöller diagram in figure 2*g*,*h*). For positive values of T_x, the jets drift to the south (the opposite is true for negative values of T_x). The drift speed remains nearly constant with time, as the pathlines created with jet positions at different times are almost straight. Similar to the tilt angle, the drift speed also increases with the bottom slope. In the reference solutions, the drift speeds are approximately 0.20, 0.48 and 0.74 cm s^{-1}, respectively. In order to compute the exact jet drift velocities in the reference solutions, we applied the principal component (PC) analysis (Hannachi, Jolliffe & Stephenson 2007) to the full flow and decomposed the velocity streamfunction field into a set of spatially coherent and temporally uncorrelated patterns. The first two empirical orthogonal functions (EOFs) are in quadrature and capture the drifting jets. The power spectra of the corresponding PCs have narrow peaks at the single frequency corresponding to the drift velocity (figure 3). The peak frequency ω and the wavevector $\boldsymbol{k} = (2\pi/L_x)\hat{\boldsymbol{i}} + (2\pi n/L_y)\hat{\boldsymbol{j}}$ (n is the number of jet pairs in the simulations, and $\hat{\boldsymbol{i}}$ and $\hat{\boldsymbol{j}}$ are the zonal and meridional unit vectors, respectively) corresponding to the jets are then used to compute the drift velocity $\boldsymbol{c} = (\omega/|\boldsymbol{k}|)\boldsymbol{k}$. We also verified that the tilt angles and drift speeds are independent of the numerical model resolution and domain size.

https://doi.org/10.1017/jfm.2018.260 Published online by Cambridge University Press

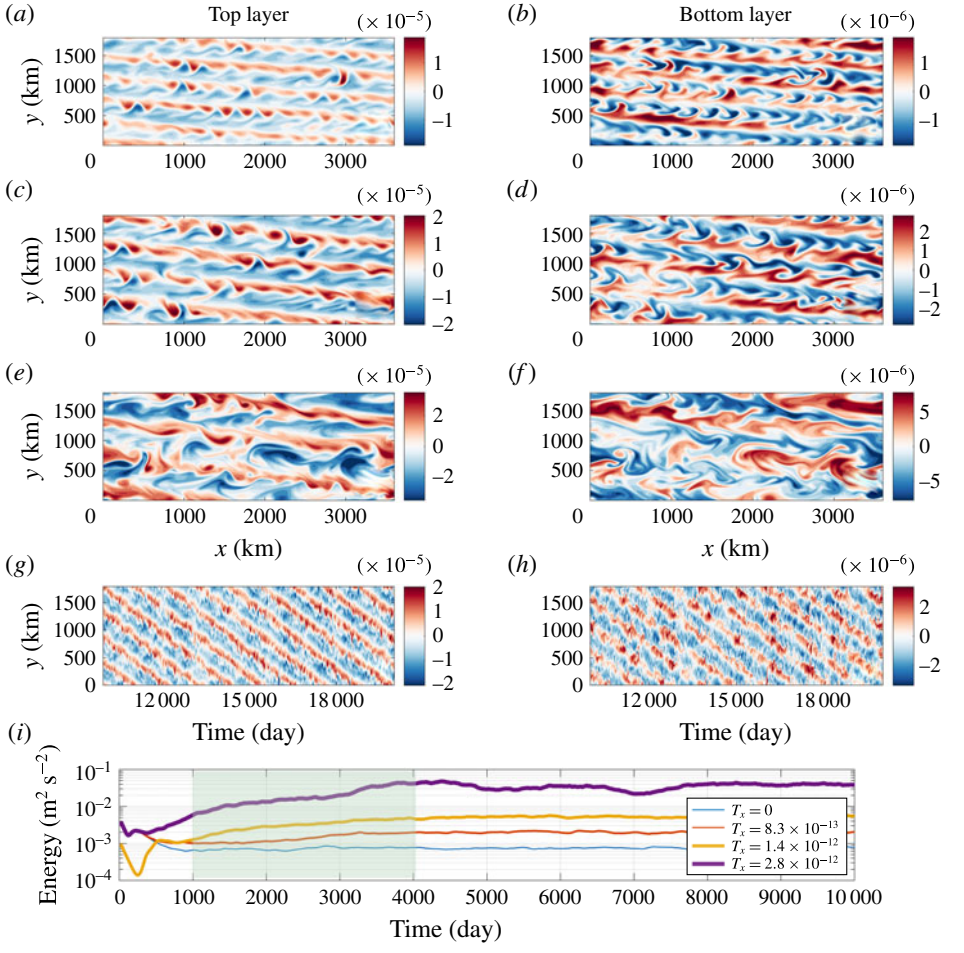


FIGURE 2. (Colour online) General flow patterns and equilibration of the jets. (*a–f*) Snapshots of the PV anomaly (colour bar units are in s^{-1}) field in the top layer ($\nabla^2\psi_1 + S_1(\psi_2 - \psi_1)$) and bottom layer ($\nabla^2\psi_2 + S_2(\psi_1 - \psi_2)$) from three reference solutions (values of T_x are given in § 2.1). (*g*,*h*) Hovmöller diagram of the PV anomaly field in the top and bottom layers (PV along a cross-section at the centre of the domain is plotted against time for the medium-slope simulation). (*i*) Total energy time series for different values of T_x (energy time series for a flat bottom case $T_x = 0$ is shown for reference). The jets tilt at angles 5.71°, 7.13° and 9.46° and drift southwards with speeds 0.20, 0.48 and 0.74 cm s^{-1}, respectively.

Even though the jets are well formed by 1000 days, the total energy of the system continuously increases until approximately 4000 days, when it reaches a statistical equilibrium. The total equilibrated flow energy $(1/2A)\int_A [H_1|\nabla\psi_1|^2 + H_2|\nabla\psi_2|^2 + H_1S_1(\psi_1 - \psi_2)^2]$ (where A is the area of the domain, and note that $H_1S_1 = H_2S_2$) increases with zonal slope (figure 2*i*). We also found tilted, drifting jets in numerical simulations in a channel configuration, where partial-slip boundary conditions were imposed on the northern and southern boundaries. The details are given in appendix A. The presence of boundaries makes the dynamics more complex, as secondary circulations are created along the boundaries. However, we do not focus on those effects in this work and restrict ourselves to periodic domains.

https://doi.org/10.1017/jfm.2018.260 Published online by Cambridge University Press

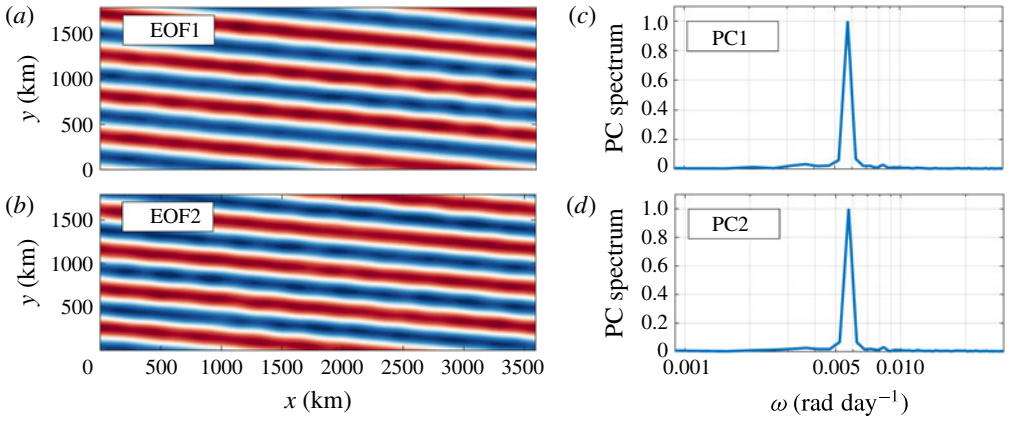


FIGURE 3. (Colour online) Principal component analysis of the streamfunction field from the medium-slope simulation: (*a*,*b*) EOF 1, 2 in the top layer (colour bar range is $[-1,\ 1]$); (*c*,*d*) power spectra of PCs (normalised to unity) corresponding to the first two EOFs. Drifting jets are analogous to a propagating wave, and two EOFs, which are identical but with a phase shift of $\pi/2$, are sufficient to represent the wave. PCs corresponding to these EOFs continuously oscillate between the maximum and minimum values to reflect the propagation of the jets; thus, their power spectra show peaks at a definite frequency. Since the wavevector $\boldsymbol{k}$ and peak frequency ω corresponding to the EOFs are known, the drift velocity of the jets can be computed as $\boldsymbol{c} = (\omega/|\boldsymbol{k}|)\boldsymbol{k}$.

We observed only three to five pairs of jets for the choice of parameter values. This is problematic in the sense that there are limited tilt angles allowed by the periodic boundaries. Given this, the tilt angles in the simulations may have been overestimated, which would then affect the drift speeds. This effect can be minimised by using a very large domain, which would increase the number of jet pairs in the system. However, that would be computationally too expensive to simulate. Nevertheless, the choice of a periodic domain does not affect the final conclusion of the paper, as our aim here is only to study the drift mechanism, and not to associate tilt angles and drift speeds with topographic slope magnitudes.

3.1. *Drift velocities from the linear dispersion relation*

Although the jet tilting is associated with the tilting of barotropic PV isolines, it is not clear why the jets drift in the presence of a zonal component of PV gradient. In order to address this aspect, we analysed the dispersion relation derived from the two-layer QG model (from (2.1) and (2.2), see appendix B for details) and found frequencies (real parts of the eigenvalues) for eigenmodes matching the jets in the reference solutions. The eigenmodes possess non-zero frequencies, which means that they propagate. The corresponding phase velocities are then compared with the drift velocities estimated from the reference solutions (table 1). The predictions from the dispersion relation are quite close to the fully nonlinear solutions, although the nonlinearities seem to slow the jets down, as the observed drift speeds are slightly smaller than the linear predictions. The difference increases with zonal slope and is almost 30 % in the large-slope simulation. On the basis of these comparisons, we conclude that the linear dispersion relation can be used to predict jet drift speeds, at least for mild zonal slopes. However, the prediction from the linear dispersion relation

https://doi.org/10.1017/jfm.2018.260 Published online by Cambridge University Press

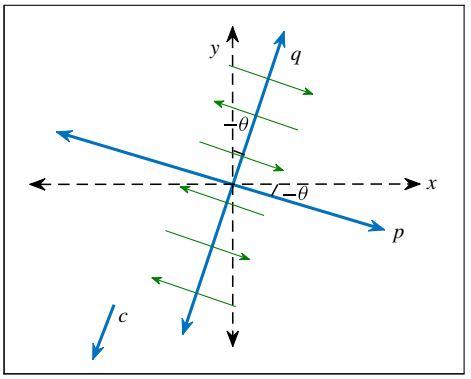


FIGURE 4. (Colour online) Sketch of the new coordinate system (new axes are p and q) that is rotated by an angle θ (tilt is positive for anticlockwise rotation) and is moving with a speed c (drift speed, positive in q direction). Angle θ and speed c are directly estimated from the numerical solutions. Green arrows represent the alternating jets; note that the time-mean profile of the jets is a function of q only.

T_x (m^{-1} s^{-1})	Drift: simulations	Drift: dispersion relation
8.3×10^{-13}	$-0.02\hat{\boldsymbol{i}} - 0.21\hat{\boldsymbol{j}}$	$-0.02\hat{\boldsymbol{i}} - 0.23\hat{\boldsymbol{j}}$
1.4×10^{-12}	$-0.06\hat{\boldsymbol{i}} - 0.47\hat{\boldsymbol{j}}$	$-0.06\hat{\boldsymbol{i}} - 0.53\hat{\boldsymbol{j}}$
2.8×10^{-12}	$-0.12\hat{\boldsymbol{i}} - 0.73\hat{\boldsymbol{j}}$	$-0.18\hat{\boldsymbol{i}} - 1.06\hat{\boldsymbol{j}}$

TABLE 1. Comparison of drift velocities (cm s^{-1}) in the numerical simulations and dispersion relation. Overall, the comparison is good but there is a systematic difference for steeper slopes. $\hat{\boldsymbol{i}}$ and $\hat{\boldsymbol{j}}$ are the zonal and meridional unit vectors, respectively.

does not work very well in cases where $O(T_x) \to O(\beta)$. This comparison is possible because linear dynamics governs a major part of the flow, and the jets correspond to the eigenmodes, which are solutions of the linear problem (Berloff & Kamenkovich 2013*a*,*b*). The main difference is that, unlike zonal eigenmodes over a flat bottom, tilted eigenmodes are not steady but propagate with constant velocities. As we show in the next section, eddies also contribute to the drift by slowing the jets down.

3.2. *Nonlinear effects and the role of eddies*

In the case of purely zonal and stationary jets, the flow can be Reynolds-style decomposed into the time-mean large-scale flow and transient eddies, and the time-mean (or zonally averaged) meridional profiles of nonlinear eddy stress terms can be analysed (e.g. Panetta 1993; Berloff *et al.* 2009*a*). Through a continuous baroclinic instability process, the eddies gain energy from the available potential energy of the system and interact with the jets via exchanges of momentum and PV, and one can study this process by comparing and correlating cross-jet profiles of the eddy forcing and time-mean PV. However, in the case of drifting jets, the analysis is not that straightforward, as the mean state itself is time-dependent. To overcome this problem, we used a new frame of reference in which the jets are stationary and aligned with one of the coordinates. In the new configuration, shown in figure 4, the frame of reference is rotated by the jet tilt angle θ and moves with a

https://doi.org/10.1017/jfm.2018.260 Published online by Cambridge University Press

constant speed c (equal to the jet drift speed). Note that PV conservation holds true irrespective of the frame of reference, as long as there is no additional acceleration. Thus, the governing equations (2.1) and (2.2) can be rewritten in the new frame of reference and interpreted as PV conservation laws (note that $\psi_i = \psi_i(p, q, t)$):

$$\left[\frac{\partial}{\partial t} - c\frac{\partial}{\partial q}\right]\Pi_1 = -\left(\frac{\partial \psi_1}{\partial p} - U_b \sin\theta\right)\frac{\partial \Pi_1}{\partial q} + \left(\frac{\partial \psi_1}{\partial q} - U_b \cos\theta\right)\frac{\partial \Pi_1}{\partial p} + \nu\nabla^4\psi_1, \tag{3.1}$$

$$\left[\frac{\partial}{\partial t} - c\frac{\partial}{\partial q}\right]\Pi_2 = -\frac{\partial \psi_2}{\partial p}\frac{\partial \Pi_2}{\partial q} + \frac{\partial \psi_2}{\partial q}\frac{\partial \Pi_2}{\partial p} + \nu\nabla^4\psi_2 - \gamma\nabla^2\psi_2, \tag{3.2}$$

where

$$\left.\begin{aligned}\Pi_1 &= \overbrace{\nabla^2\psi_1 + S_1(\psi_2 - \psi_1)}^{Q_1} + (\beta + S_1U_b)(q\cos\theta + p\sin\theta + ct\cos\theta),\\ \Pi_2 &= \overbrace{\nabla^2\psi_2 + S_2(\psi_1 - \psi_2)}^{Q_2} + (\beta - S_2U_b)(q\cos\theta + p\sin\theta + ct\cos\theta)\\ &\quad + T_x(-q\sin\theta + p\cos\theta - ct\sin\theta).\end{aligned}\right\} \tag{3.3}$$

Here, Π_i represents the absolute PV (i.e. the sum of PV due to the generated flow Q_i and the background PV) in individual layers. Also note that all variables are functions of p, q, t and $\boldsymbol{\nabla} = (\partial/\partial p, \partial/\partial q)$. The first two terms on the right-hand side of (3.1) and (3.2) contain both linear and nonlinear terms, which are due to the background PV gradients, generated flow and nonlinear eddy effects. Depending on the overall sign of the sum, Q_i can be forced or damped, resulting in strengthening or weakening of the jets. The rest of the terms on the right-hand side always smooth the PV gradients by removing energy from the system through viscous dissipation and bottom drag. In order to understand the effects of eddies and linear terms, we derived the time-mean equations from (3.1) and (3.2) by representing the variables as a sum of the time-mean flow ($\overline{Q}_i$, $\overline{\psi}_i$) and time-dependent eddy field (Q_i', ψ_i'). This is basically the Reynolds flow decomposition in the moving frame of reference. The equations are then averaged over time (see full derivation in appendix C):

$$\frac{\partial \overline{Q}_1}{\partial t} = \underbrace{-\boldsymbol{\nabla}\cdot\overline{(\boldsymbol{u}_1'Q_1')}}_{\text{eddy forcing}} + \underbrace{\overbrace{(c + U_b\sin\theta)\frac{\partial \overline{Q}_1}{\partial q}}^{L_1^c} \overbrace{- (\beta + S_1U_b)\sin\theta\ \overline{u}_1}^{L_1^m}}_{\text{linear stress terms}} + \underbrace{\overbrace{\nu\nabla^2\overline{\zeta}_1}^{D_1^\nu}}_{\text{dissipation}}, \tag{3.4}$$

$$\frac{\partial \overline{Q}_2}{\partial t} = \overbrace{-\boldsymbol{\nabla}\cdot\overline{(\boldsymbol{u}_2'Q_2')}}^{\text{eddy forcing}} + \underbrace{c\frac{\partial \overline{Q}_2}{\partial q}}_{L_2^c} \overbrace{\underbrace{- [(\beta - S_2U_b)\sin\theta + T_x\cos\theta]\,\overline{u}_2}_{L_2^m} + \underbrace{\nu\nabla^2\overline{\zeta}_2}_{D_2^\nu} \underbrace{- \gamma\overline{\zeta}_2}_{D_2^\gamma}}^{\text{linear stress terms}}, \tag{3.5}$$

where $\boldsymbol{u}_i$ is the new velocity ($\boldsymbol{u}_i = (u_i, v_i) = (-\partial\psi_i/\partial q, \partial\psi_i/\partial p)$) and ζ_i is the new relative vorticity ($\zeta_i = \nabla^2\psi_i$) in each layer. Here, we retain the time derivatives in the time-mean PV (in the rest of the paper, 'mean PV' refers to the mean PV of the developed flow only i.e. $\overline{Q}_i$), but the terms vanish in the steady state and are kept here only for clarity. As seen in (3.4) and (3.5), the nonlinear terms (referred

https://doi.org/10.1017/jfm.2018.260 Published online by Cambridge University Press

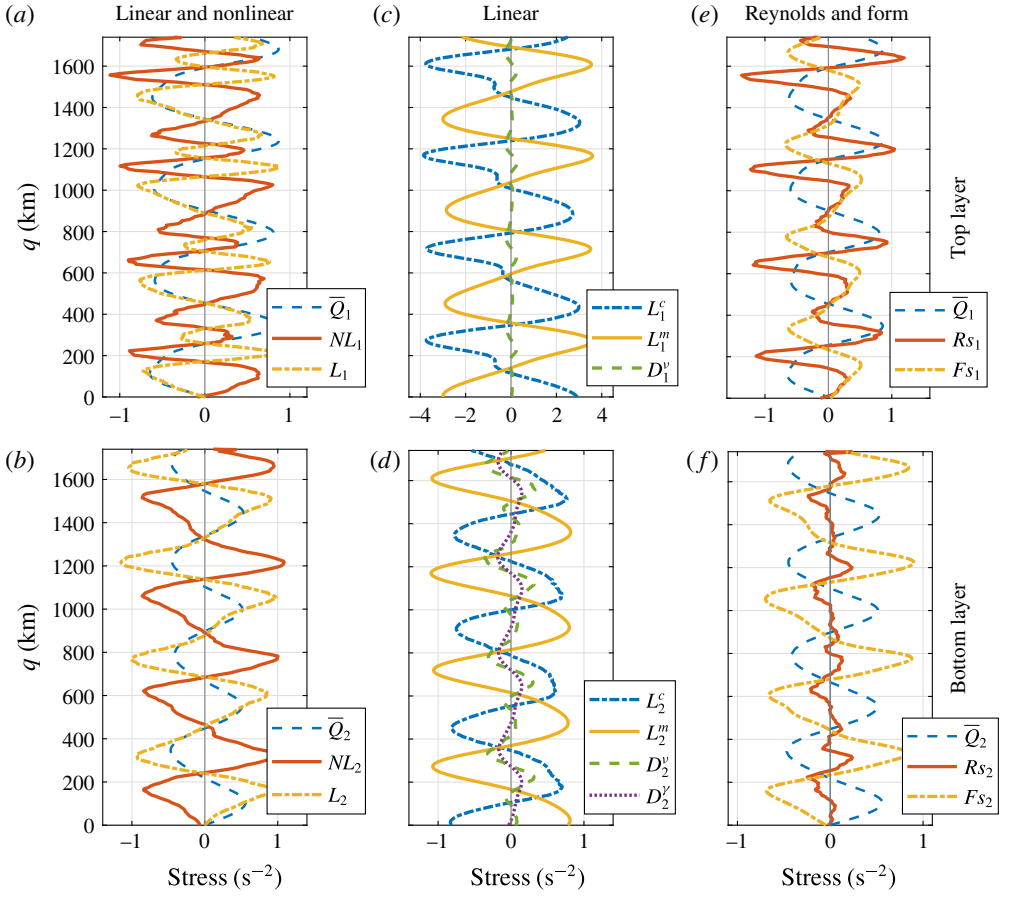


FIGURE 5. (Colour online) Cross-jet profiles for the medium-slope simulation averaged in the moving frame in the interval 10 000–20 000 days. (*a*,*b*) Eddy forcing (NL_i, smoothed with 10-point moving average) and linear stress terms plus dissipation terms (L_i). (*c*,*d*) Radiation stress term, inertial stress term and dissipation terms. (*e*,*f*) Reynolds stress term and form stress term (smoothed with 10-point moving average). Top and bottom rows are for the top and bottom layers, respectively. In order to normalise the plots, the stress terms (units are in s^{-2}) are multiplied by factors of 5×10^{12} and 2×10^{13} in the top and bottom layers, respectively. Dashed blue curves in (*a*,*b*,*e*,*f*) represent the time-mean PV profiles ($\overline{Q}_i$, normalised), which are multiplied by factors of 2.2×10^5 and 8.8×10^5 in the top and bottom layers, respectively. The eddies act against the jets, whereas the jets are forced by the linear stress terms.

to hereafter as 'eddy forcing' or 'nonlinear stress term') and the linear terms ('linear stress terms' $L_i^c + L_i^m$, and 'dissipation terms' $D_i^\nu + D_i^\gamma$) balance each other in the stationary equilibrated state.

In order to compute the eddy forcing and linear stress terms, we first linearly interpolated the streamfunction field on a rectangular grid rotated by the jet tilt angle θ and aligned the streamfunction snapshots in the moving frame of reference at every time step. We then computed the stress terms using the relations (3.4) and (3.5) and averaged them over time and along the jets. Cross-jet profiles of these linear and nonlinear stress terms for the medium-slope solution are shown in figure 5. As expected from the equations, the linear and nonlinear stress terms

https://doi.org/10.1017/jfm.2018.260 Published online by Cambridge University Press

Layer	Linear $(L_i^c + L_i^m)$	Eddy $(Rs_i + Fs_i)$	Reynolds (Rs_i)	Form (Fs_i)
Top $(i = 1)$	0.60	−0.24	0.26	−0.93
Bottom $(i = 2)$	0.86	−0.33	−0.01	−0.89

TABLE 2. Correlation coefficients between cross-jet profiles of the time-mean linear and nonlinear stress terms, and the time-mean PV $(\overline{Q}_i)$ in both layers for the medium-slope simulation. The linear stress terms support the jets, whereas the eddy forcing opposes them.

balance each other (figure 5*a*,*b*). (There are small deviations from zero due to the data interpolation. An interpolation scheme with higher-order accuracy could be used, but we found linear interpolation to be sufficient for our purposes. In fact, we also computed the stress terms in the original xy coordinate system and interpolated the stress field, but the resulting differences were found to be insignificant.) Relative contributions of the individual linear terms are also analysed (see figure 5*c*,*d*): the L^c and L^m terms (hereafter referred to as 'radiation stress term' and 'inertial stress term', respectively) in the top layer are almost four times larger in magnitude than the eddy forcing, whereas all these terms are of comparable strength in the bottom layer. In the top layer, the radiation and inertial stress terms largely balance each other, and the difference between them is compensated by the eddy forcing. In both layers, the dissipation terms are significantly small and can be safely neglected. In terms of kinetic energy, the top layer dominates over the bottom layer and is two to three times more energetic (not shown). Thus, this supports the hypothesis that linear modes control a major part of the flow dynamics and hence the drift.

It is important to note that the eddy forcing tends to smooth the mean PV profile in both layers and counteract the linear stress terms (figure 5*a*,*b*). We computed correlation coefficients between the cross-jet profiles of the time-mean PV and stress terms. The linear stress terms are positively correlated (correlation coefficients ~ 0.6) with the time-mean PV, whereas the eddy forcing terms show negative correlation (~ -0.3) with the time-mean PV (table 2). This is in contrast to previous studies on oceanic jets (Berloff *et al.* 2009*a*,*b*; Chen *et al.* 2015) and jets in planetary atmospheres (Ingersoll *et al.* 1981; Panetta 1993; Ingersoll *et al.* 2000), where the jets are essentially eddy-driven. To clarify this matter, we decomposed the eddy forcing into the Reynolds stress term (Rs) and form stress term (Fs):

$$Rs_i = -\boldsymbol{\nabla} \cdot \overline{(\boldsymbol{u}_i' \zeta_i')}, \tag{3.6}$$

$$Fs_i = -\epsilon_i S_i \boldsymbol{\nabla} \cdot \overline{(\boldsymbol{u}_i' (\psi_2' - \psi_1'))}, \tag{3.7}$$

where $\epsilon_1 = -\epsilon_2 = 1$, and $i = 1, 2$ for the top and bottom layers, respectively. Note that the Reynolds stress term and form stress term are simply the convergence of eddy fluxes of relative vorticity and buoyancy, respectively. As shown in figure 5(*e*,*f*), the form stress term tends to smooth the PV gradients (correlation coefficients between the form stress term and mean PV profiles are ~ -0.9 in both layers); hence, the form stress term opposes the jets. On the other hand, the Reynolds stress term shows a positive (no) correlation with the mean PV in the top (bottom) layer, which means that only the upper-layer Reynolds stress term forces the jets – see also the discussion in Thompson & Young (2007). The former observation is comforting in terms of theoretical aspects, because the form stress term is expected to be against

https://doi.org/10.1017/jfm.2018.260 Published online by Cambridge University Press

the mean PV in a baroclinically unstable flow system forced with an eastward background flow (Berloff *et al.* 2009*a*). The Reynolds stress term and form stress term are comparable in magnitude in the top layer; however, in the bottom layer, the magnitude of the Reynolds stress term is quite small in comparison to the form stress term, and the effect of the form stress term is more prominent. In the absence of topography, the Reynolds stress term, which is responsible for maintaining the jets in the eastward background shears, dominates over the form stress term and, overall, the eddy forcing is positively correlated with the mean PV. However, here, in the presence of zonal bottom slope, the form stress term overcomes the Reynolds stress term and the overall impact of the eddies is the opposite. This is also in agreement with the linear predictions, which say that any zonal variation in bottom topography enhances the baroclinic instability (Hart 1975; Chen & Kamenkovich 2013). In a study of the North Atlantic jets, Kamenkovich, Berloff & Pedlosky (2009) also found both kinds of eddy feedbacks (see also Melnichenko *et al.* 2010; Barthel *et al.* 2017; Youngs *et al.* 2017). It is important to note that, if the eddy field is computed by high-pass time filtering in a stationary frame of reference, then the resulting eddy field would also include the drifting jets. Thus, the eddy forcing would include terms interpreted as linear stress terms in this study. This may complicate comparison between our work and some earlier studies.

We also analysed the cross-jet profiles of the eddy PV fluxes $\overline{v_i' Q_i'}$, relative vorticity fluxes $\overline{v_i' \zeta_i'}$ and buoyancy fluxes $\epsilon_i S_i \, \overline{v_i'(\psi_2' - \psi_1')}$ across the jets (figure 6*a*,*b*). The eddy PV fluxes have most of the contribution from the eddy buoyancy fluxes (also referred to as 'eddy heat fluxes'), which are uniformly negative (positive) in the top (bottom) layer. In order to understand the role of the eddy buoyancy fluxes, we computed the eddy heat diffusivity μ_h,

$$\mu_h = \frac{\epsilon_i S_i \, \overline{v_i'(\psi_2' - \psi_1')}}{-\partial_q \overline{b}_i} = \frac{\epsilon_i S_i \, \overline{v_i'(\psi_2' - \psi_1')}}{-\partial_q(\epsilon_i S_i(\overline{\psi}_2 - \overline{\psi}_1) + \epsilon_i S_i U_b q \cos\theta)} = \frac{\overline{v_i'(\psi_2' - \psi_1')}}{\overline{u}_2 - \overline{u}_1 - U_b \cos\theta}, \tag{3.8}$$

where $\overline{b}_i$ represents the time-mean buoyancy in the layer. Note that the notation is the same as in (3.6) and (3.7). Although the heat diffusivity relations are different in the top and bottom layers, they are mathematically equivalent and would result in the same cross-jet profile of the heat diffusivity in both layers. As shown in figure 6(*c*), the heat diffusivity is positive everywhere. This means that the eddies advect buoyancy anomaly in the direction of decreasing $\overline{b}$, resulting in the smoothing of mean PV gradients, or, in other words, the eddy buoyancy fluxes are down-gradient. The minima in the eddy heat diffusivity profile coincide with the westward jets, whereas the eddy heat diffusivity is strongest just south of the eastward jets. Since the largest eddy flux covers the eastward jet core, the dynamics is profoundly different from the barotropic 'PV staircases' characterised by partial eddy transport barriers located on the eastward jet cores (e.g. Dritschel & McIntyre 2008). Also, the magnitude of the eddy heat diffusivity increases with zonal slope. On the other hand, the eddy relative vorticity fluxes force the jets (figure 6*a*,*b*), as they are strongly correlated with the mean flow (see expression (15.21) in Vallis 2017). Since eddy heat diffusivity and PV diffusivity are not the same, eddy PV diffusivity was also computed in each layer and the PV diffusivity magnitudes were found to be largely positive. Overall, the eddy buoyancy fluxes dominate over the eddy relative vorticity fluxes; hence, the eddy PV fluxes are down-gradient. The roles of these fluxes are the same, as in the case of stationary zonal jets (Panetta 1993; Thompson & Young 2007), and only the relative magnitudes of the relative vorticity and buoyancy fluxes change because of the zonal asymmetry.

https://doi.org/10.1017/jfm.2018.260 Published online by Cambridge University Press

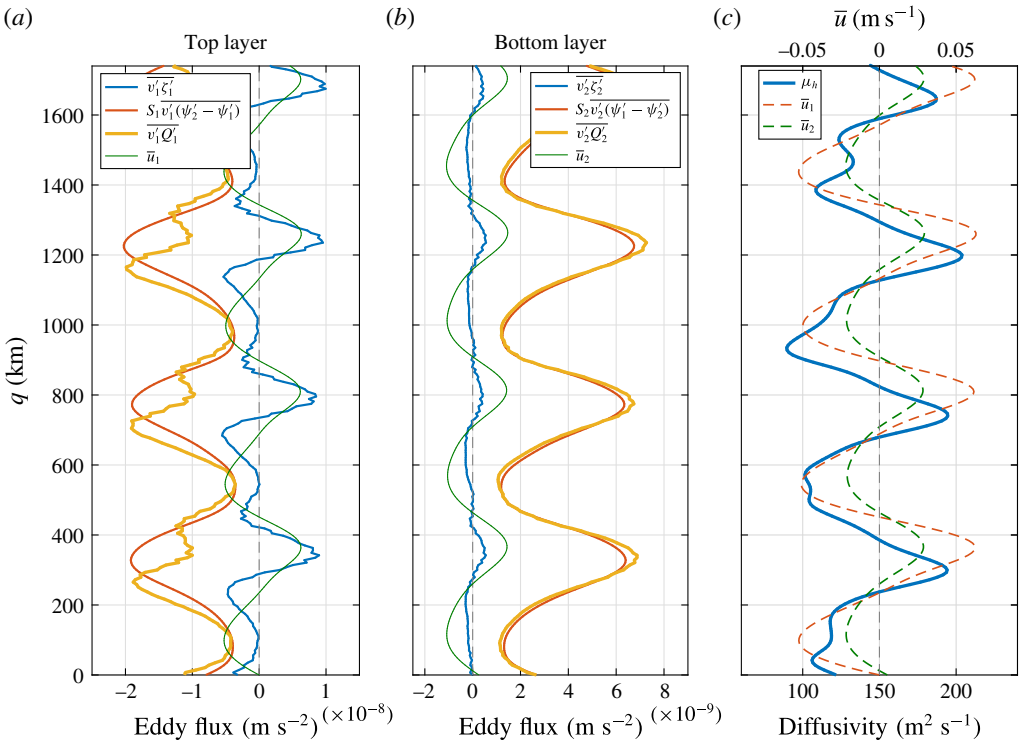


FIGURE 6. (Colour online) Cross-jet profiles for the medium-slope simulation averaged in the moving frame in the interval 10 000–20 000 days. (*a*,*b*) Eddy PV flux $\overline{v_i'Q_i'}$, eddy relative vorticity flux $\overline{v_i'\zeta_i'}$ and eddy buoyancy flux $\epsilon_i S_i\,\overline{v_i'(\psi_2'-\psi_1')}$ across the jets (smoothed with 10-point moving average). (*c*) Heat diffusivity. The thin green curves in (*a*,*b*) represent the mean flow (normalised) in individual layers, and actual magnitudes of the velocities are shown in (*c*).

Given this, there must exist a critical value of zonal slope where the effects of the Reynolds stress term and form stress term exactly counter each other, and eddies start to oppose the jets beyond that critical slope. We computed correlation coefficients between the eddy forcing and mean PV profiles in simulations with different zonal slope magnitudes (table 3). Over a flat bottom, jets are supported by the eddy forcing and this is clearly captured by a strong positive correlation in the top layer for $T_x = 0$. As the zonal slope increases, the eddy forcing correlation coefficient in the top layer changes sign from positive to negative. On the other hand, correlation coefficients in the bottom layer are negative in all cases. This is mostly because only the upper-layer Reynolds stress term is responsible for maintaining the jets (Thompson & Young 2007), whereas the lower-layer Reynolds stress term is small in magnitude and does not have any significant effect (see figure 5*f*). It should be noted that the critical slope value computed here is not unique, and it would differ in different parameter regimes. Moreover, periodic boundary conditions may also affect the value of critical slope.

Looking at both the eddy forcing and eddy PV fluxes, we conclude that the vertical structure plays a significant part in deciding the role of eddies. Oceanic eddies are complex, as they can either force or damp a large-scale circulation. The primary role of the eddies is to stabilise the system and bound the alternating jets. In the case of

https://doi.org/10.1017/jfm.2018.260 Published online by Cambridge University Press

T_x (m^{-1} s^{-1})	0	5.53×10^{-13}	8.3×10^{-13}	1.4×10^{-12}	1.94×10^{-12}	2.8×10^{-12}
Top $(Rs_1 + Fs_1)$	0.67	0.24	−0.07	−0.24	−0.64	−0.56
Bottom $(Rs_2 + Fs_2)$	−0.52	−0.82	−0.84	−0.33	−0.97	−0.66

TABLE 3. Correlation coefficients between the cross-jet profiles of the time-mean nonlinear stress terms, and the time-mean PV ($\overline{Q}_i$) in both layers in different simulations (all parameters were kept the same, as given in § 2.1, except T_x). As the zonal slope is increased, eddies change their behaviour from being jet-supporting to jet-opposing.

	L_i^c			L_i^m		
Layer	Cor.	Min. lag-cor.	Lag (deg.)	Cor.	Max. lag-cor.	Lag (deg.)
Top $(i = 1)$	0	−0.91	84.37	0.13	0.97	78.75
Bottom $(i = 2)$	0	−0.97	90	0.58	0.97	56.25

TABLE 4. Correlation coefficients and maximum/minimum lag-correlation coefficients between the time-mean cross-jet profiles of the linear stress terms and the time-mean PV ($\overline{Q}_i$) in both layers for the medium-slope simulation. Here, the lag period of 2π is equivalent to the meridional width of one pair of jets.

a flat bottom, eddies force the jets and compensate for the energy removed through dissipation. The bounding mechanism is due to over-localisation of the eddies and the resulting loss of the eddy forcing efficiency (Berloff *et al.* 2011). In contrast, in the presence of zonal slope, the jets are no longer parallel to the imposed background flow and can be directly forced by the vertical shear, as seen in the inertial stress term L^m. Here, the eddies act against the jets to balance the linear forcing, so that the jets can be stabilised and bounded.

3.3. *Jet drift mechanism*

The analysis in the previous sections predicts that the linear dynamics controls the jet drift. In order to understand this physically, the linear stress terms in expressions (3.4) and (3.5) need to be examined more carefully. Here, the inertial stress term, which is the forcing term for the mean PV, is proportional to the developed mean flow. By construction, the maxima of the mean along-jet velocity and mean PV profiles do not align and are significantly offset. Similarly, the radiation stress term, which partially compensates against the inertial stress term, is also significantly shifted and, in fact, exactly orthogonal to the mean PV profile (i.e. zero correlation), as it is proportional to the first derivative of $\overline{Q}_i$ (see table 4 for the maximum/minimum correlation coefficients and corresponding lead/lag phases). In contrast, the eddy forcing maxima are almost aligned with the mean PV maxima, and there is a negligible improvement in correlations with the time-lagged profiles (table 5). The maximum increase in local PV occurs at the locations of the along-jet velocity maxima (figure 7). To account for PV conservation along with this local PV increase, the jets drift southwards. In other words, the off-core linear forcing pushes the jets in the meridional direction. The same is true for northward drifting jets in the case of a negative zonal slope, where the relative shifts between the mean PV and mean flow are simply reversed.

The drift mechanism also agrees with the hypothesis by Boland *et al.* (2012). They suggest that the jet drift is a result of PV conservation, and the along-jet PV advection

https://doi.org/10.1017/jfm.2018.260 Published online by Cambridge University Press

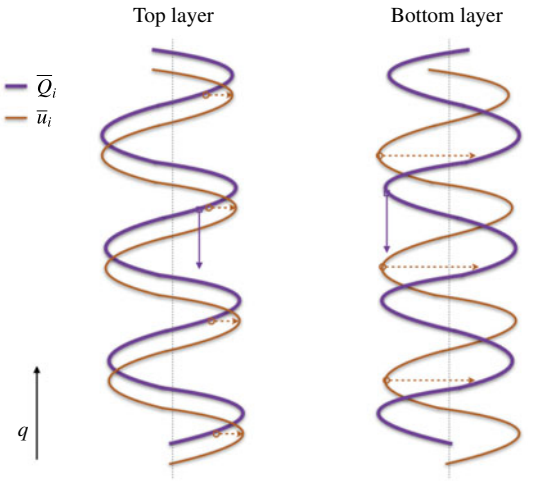


FIGURE 7. (Colour online) Sketch of cross-jet profiles of the time-mean PV (blue thick) and mean flow (red-brown thin) in both layers in numerical simulations with positive zonal slopes in topography (relative magnitudes are not to scale). The maxima of the mean flow and mean PV profiles do not align, and there is a large shift. Red dashed arrows indicate the tendency of PV to increase/decrease at the velocity maxima due to the mean flow, and blue solid arrows indicate the direction of the drift. Vertical dotted lines represent the zero lines.

	Reynolds stress (Rs_i)			Form stress (Fs_i)		
Layer	Cor.	Max. lag-cor.	Lag (deg.)	Cor.	Min. lag-cor.	Lag (deg.)
Top ($i=1$)	0.26	0.29	16.87	−0.93	−0.96	11.25
Bottom ($i=2$)	−0.01	0.08	−129.37	−0.89	−0.90	−11.25

TABLE 5. Correlation coefficients and maximum/minimum lag-correlation coefficients between the time-mean cross-jet profiles of Reynolds stress term and form stress term, and the time-mean PV ($\overline{Q}_i$) in both layers for the medium-slope simulation. Here, the lag period of 2π is equivalent to the meridional width of one pair of jets.

is compensated by a meridional drift. From (3.4) and (3.5), it is clear that the inertial stress term is basically advection of a PV component by the mean flow, and the jets drift to compensate for this advection (see expression of the radiation stress term). Melnichenko *et al.* (2010) studied the role of eddy fluxes in the formation of striations in the Pacific. They also showed that linear advection terms appear in the time-averaged PV budget due to the non-zero angle between the background flow and tilted striations. Here, too, the striations tend to drift across the mean PV contours, which may be due to the presence of the linear advection terms. It is natural to ask why eddies do not stop this drift, as the eddy forcing maxima are also not aligned with the mean PV maxima in a way that would support a northward drift and counteract the southward propagation of the jets. Indeed, the eddies do tend to slow the jets down (see table 1); however, for the topographic slopes considered, the eddy effect is small and cannot overcome the drift induced by the mean flow. On the other hand, the eddy effect may be significant for steeper slopes, which was seen in Thompson & Richards (2011) and Chen *et al.* (2015).

https://doi.org/10.1017/jfm.2018.260 Published online by Cambridge University Press

It is important to note here that a sloping topography is not the only way to generate drifting jets, which are also observed in systems forced with a meridionally non-uniform stress term (Williams 2003; Chan, Plumb & Cerovecki 2007; Chemke & Kaspi 2015*b*). In these systems, the drift cannot be explained by the off-core linear forcing mechanism described above, which is only valid for tilted, drifting jets over topography, and is thought to be caused by meridionally asymmetric eddy momentum fluxes or a residual flow in the meridional direction. Srinivasan (2013) suggests that the jet drift in general is caused by the breaking of reflectional (or mirror) symmetry in a system. Most of the studies that use idealised models on the β-plane are forced with either a uniform zonal flow or an isotropic small-scale random forcing. These choices preserve the mirror symmetry and, thus, generate steady zonal jets. The mirror symmetry can be broken, even in a barotropic model, e.g. by using an anisotropic forcing term, and in response drifting jets can be formed (see chap. 3 in Srinivasan 2013). In our study, the mirror symmetry is broken by the zonal slope in topography, resulting in drifting jets. However, there are differences between these two scenarios. The drift mechanisms are different in these two cases, and also, the drifting jets with anisotropic forcing are purely zonal, whereas the jets formed over zonally sloping topography are tilted. The concept of the mirror symmetry can potentially predict the drifting behaviour in various systems, but it is not clear, whether it can be also quantitative.

3.4. *Interpreting the linear forcing*

In the presence of a zonally sloping topography, the jets are maintained by the inertial stress term, which is proportional to the mean flow, and the eddies act against the jets. It is very tempting to assume here that the forcing is due to the mean flow itself; however, that is not feasible according to the laws of physics. The jets cannot force themselves and simultaneously lose energy to the eddies. Here, the jets are directly forced by the imposed vertical shear in the presence of the zonal slope, and the intensity of the linear forcing depends on the mean flow itself. The zonal bottom slope acts like a coupling between the tilted jets and background flow, and the jets gain energy directly from the background flow. This balance between the jets and eddies only works in forced dissipative turbulent systems. If the background flow and dissipation terms were removed, the jets would dissipate and lose all their energy to eddies, thus leading to a very different flow dynamics. However, a detailed analysis of that is beyond the scope of this paper and is being pursued as a separate piece of work.

3.5. *Energy equilibration and the long-time flow adjustment*

In addition to tilting and drifting of the jets, another difference made by the zonal component of PV gradient is that there is a significant increase in the equilibrated energy of the system (figure 2*e*). Arbic & Flierl (2004) showed that the eddy energy of the equilibrium state greatly increases when the vertical shear is oriented not in the east–west direction. The increase is proportional to the angle between the direction of the vertical shear and PV isolines (see also Smith 2007). In this work, we tilt the PV isolines by introducing the zonal slope in bottom topography, which basically introduces a non-zero angle between the background PV and vertical shear, and thus increases the energy of the equilibrated state. This can also be understood by analysing the eddy field. In the presence of the zonal slope, eddies grow through baroclinic instability (by extracting energy from the imposed background shear) and also gain energy from the mean flow itself, i.e. the jets in this case. In this situation, both the jets and eddies tend to be more energetic.

https://doi.org/10.1017/jfm.2018.260 Published online by Cambridge University Press

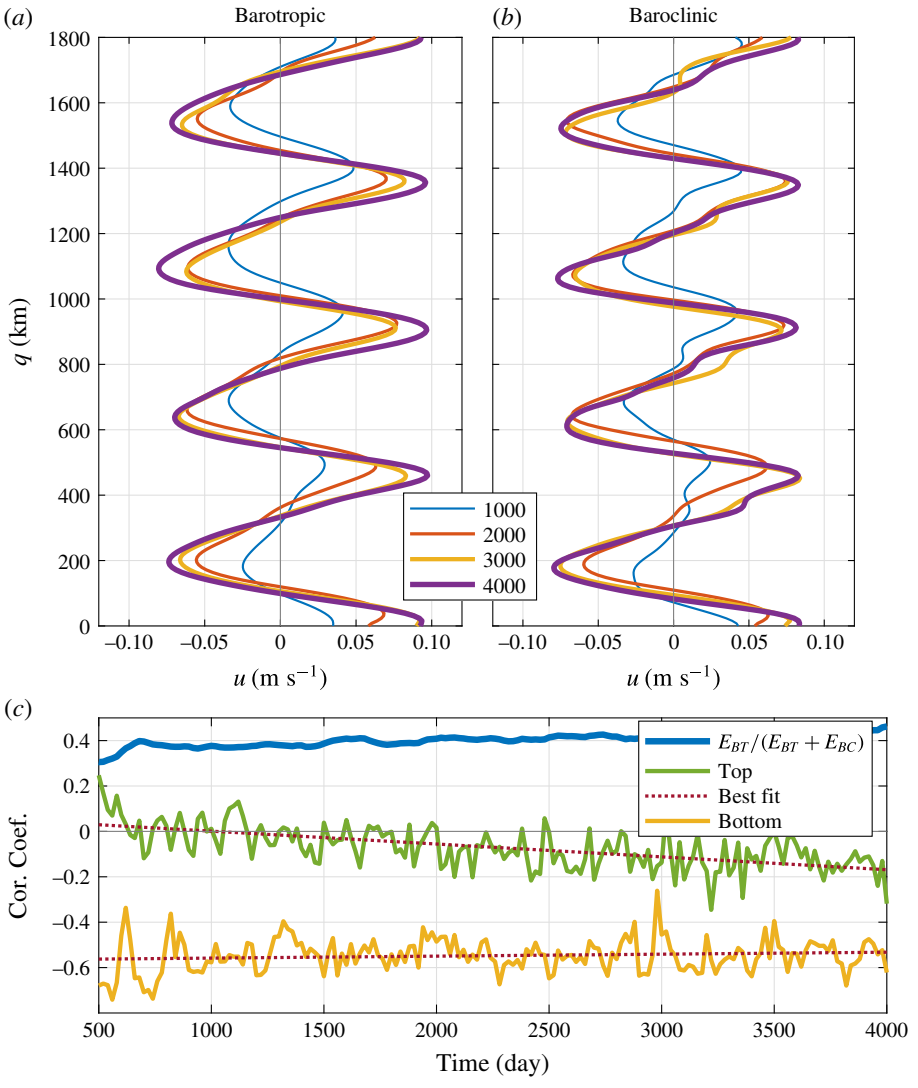


FIGURE 8. (Colour online) Flow properties in the transient state of the medium-slope solution. The time evolutions of: (*a*) barotropic velocity $= (1/(H_1 + H_2))(H_1u_1 + H_2u_2)$; (*b*) baroclinic velocity $= u_1 - u_2$ (cross-jet profiles, averaged along the jets, are aligned in the moving frame of reference by assuming a constant drift velocity; note that legend units are in days); and (*c*) correlation coefficients between the cross-jet profiles of eddy forcing and PV, and the fraction of the total energy in the barotropic component. Here, we used the full flow field to compute the eddy forcing, because it was not possible to compute a mean flow in the transient state.

Moreover, it takes a long time for the system to attain equilibrium. The continuous increase of the total energy (roughly in the interval 1000–4000 days, figure 2*e*) is definitely not during the time period when the jets are being formed (§ 2.1), but it has to do with some secondary effects. To investigate this, we first look at the time evolution of the barotropic and baroclinic velocity components in the transient period (figure 8*a*,*b*). Both the barotropic and baroclinic velocity fields increase at similar

https://doi.org/10.1017/jfm.2018.260 Published online by Cambridge University Press

rates, and, in fact, the ratio of energy in the barotropic component to the total energy (barotropic plus baroclinic, $E_{BT} + E_{BC}$) remains almost constant during this period (blue curve in figure 8*c*).

One possible explanation behind this slow energy increase could be the direct forcing by the background flow once the jets are formed. The inertial stress term depends on the mean flow; hence, the linear forcing becomes prominent only after the formation of the jets. Note that the jet formation occurs due to the upscale transfer of energy by mesoscale eddies that receive energy from the background flow. However, at a later stage, the eddies start acting against the linear stress terms and oppose the jets. So, there must be a time interval when the eddies change their behaviour from being jet-supporting to jet-opposing. To confirm this hypothesis, we computed correlation coefficients between the cross-jet eddy forcing and PV profiles during the transient period (figure 8*c*). The time evolution of the correlation coefficient shows a decreasing trend in the top layer, where the correlation coefficient changes from a small positive value to negative values with time. On the other hand, the correlation remains negative in the bottom layer. This is probably because the eddy forcing in the bottom layer is largely due to the form stress term, thus producing a negative correlation at all times (also read the discussion of table 3). The results are in accord with our hypothesis, at least in the more active top layer that offers an explanation of the long time scale in the transient period.

4. Conclusions

Interaction of oceanic jets with bottom topography is a problem of interest to many. Here, we studied the effects of zonally sloping bottom topography on the dynamics of multiple alternating jets in oceans in a forced dissipative two-layer nonlinear QG model. In accord with previous studies (Boland *et al.* 2012; Chen *et al.* 2015), the jets tilt from the zonal direction and drift. We find that the jet drift is strongly controlled by the linear dynamics. The drift velocities are predicted quite accurately with the linear dispersion relation, although the nonlinear eddy effects contribute, and more so for steeper topographic slopes. In the presence of the zonal asymmetry due to the bottom slope, the jets are able to extract energy directly from the imposed background flow, and the forcing term is directly proportional to the developed mean flow. Thus, the linear forcing and mean PV maxima do not align and have a large offset. Because of the off-core linear forcing, the jets are pushed in the meridional direction. If looked at from the point of view of PV conservation, the jets drift meridionally to compensate for the along-jet advection of PV by the mean flow, in agreement with Boland *et al.* (2012).

On the other hand, the nonlinear eddy forcing does not cause the drift; however, it influences the drift speed by modifying the effective balance between the linear terms. In order to understand the impacts of the eddies, we derived the governing equations in a tilted, non-stationary frame of reference and compared cross-jet profiles of the linear and nonlinear stress terms with the mean PV profile. Here, the eddy forcing is found to be opposing the jets, which is in contrast to the case of stationary zonal jets (Panetta 1993; Berloff *et al.* 2009*a*). The net linear stress term, present in the time-mean equations, directly forces the jets. The eddy forcing was further decomposed into the Reynolds stress term and form stress term. The behaviour of the form stress term is similar to the case of stationary zonal jets over a flat bottom, i.e. the form stress term opposes the jets (Berloff *et al.* 2009*a*). On the other hand, the Reynolds stress term in the upper layer is responsible for forcing the jets

https://doi.org/10.1017/jfm.2018.260 Published online by Cambridge University Press

(Thompson & Young 2007). Overall, the form stress term dominates and is such that the eddies remove energy from the jets. The gradual transition in the role of eddies from being jet-supporting to being jet-opposing is also confirmed by correlating the cross-jet profiles of the eddy forcing and mean PV anomalies in simulations with different zonal slope magnitudes. The same conclusion was reached when we analysed various eddy fluxes. In the presence of the topography, the eddy buoyancy fluxes oppose the jets in both layers but are much stronger in magnitude than the relative vorticity fluxes, which are jet-supporting. The eddy heat diffusivity, computed from the buoyancy fluxes, is positive everywhere and the maxima occur just south of the eastward jet cores, which may be related to the southward drift of the jets. Overall, the eddy PV fluxes are down-gradient and oppose the jets.

This is in contrast to the conventional point of view that the eddy field maintains the jets – hence the term 'eddy-driven jets'. We argue, at least in the oceans, that the eddy field can either force or oppose the jets depending on the situation (see e.g. Kamenkovich *et al.* 2009). Overall, the eddy field allows the jets to reach an equilibrium state. Thus, with regards to oceanic jets, it would be more appropriate to use a term like 'eddy-sustained jets'. This general eddy effect may not be limited to alternating jets and may be important in other large-scale oceanic flows. For example, eddies play a major role in the dynamics of the Antarctic Circumpolar Current (ACC) (Abernathey & Cessi 2014; Thompson & Naveira Garabato 2014). Recent studies have shown that the behaviour of the Reynolds stress term and form stress term can change abruptly around the topographic features in the Southern Ocean, where, in different parts of the ocean, eddies are seen to be forcing the large-scale flow as well as gaining energy via a barotropic energy source (Barthel *et al.* 2017; Youngs *et al.* 2017).

While examining the total energy of the system, we observed that the flow energy increases with the bottom slope, in agreement with earlier studies (Arbic & Flierl 2004; Smith 2007; Boland *et al.* 2012). In our study, the eddies gain energy from the baroclinically unstable background flow as well as from the jets, whereas the jets are maintained by the imposed vertical shear. Since both the jets and eddies are forced by the imposed shear, the system tends to be more energetic. It should be noted that the results discussed in this paper are limited to continuously forced dissipative systems and may not apply directly to freely evolving turbulence.

Topography also plays a crucial role in ocean mixing and transport (Tréguier & Panetta 1994; Thompson 2010). Studies on the dynamics of the Southern Ocean have shown enhanced mixing at mid-depths, which is believed to be due to interactions of jets with topography (Abernathey *et al.* 2010; Lu & Speer 2010). Idealised studies have also reported enhanced material transport across tilted, drifting jets (Boland *et al.* 2012; Stern *et al.* 2015). In fact, a more general question which should be addressed is: What are the effects of the zonal component of PV gradient on the overall dynamics? In reality, the oceans are full of zonal gradients in PV, as the ocean floor is not flat, and, also, the oceans are forced with a wind field having both zonal and meridional components. In this work, we restricted ourselves to a very simple idealised case, but numerical experiments in the presence of a realistic ocean bathymetry forced with an observed wind field are needed to understand the effects in the real oceans. Such studies would shed some light on the role of geostrophic eddies in large-scale ocean mixing and material transport in the presence of topography, and might even be helpful in incorporating topographic impacts in eddy parametrisation schemes. In addition, the effects of continental boundaries could also be analysed. Finally, our dynamical analyses are based on the Reynolds decomposition of the flow into the time-mean (in a non-stationary frame of reference) and fluctuation parts

https://doi.org/10.1017/jfm.2018.260 Published online by Cambridge University Press

of the flow, and in the future it would be useful to consider other decompositions (e.g. Berloff 2005*a*), which are more relevant for parametrising the involved eddy effects in non-eddy-resolving or eddy-permitting models. Further work related to the energetics and stability of the drifting jets is in progress and will be addressed in future.

Acknowledgements

H.K. would like to acknowledge the support from the President's Scholarship and the Mathematics of Planet Earth CDT, Imperial College. P.B. has been supported by EPSRC Mathematics Platform grant EP/I019111/1 and NERC grant NE/R011567/1. The authors thank I. Kamenkovich and two anonymous reviewers for their comments and suggestions that helped to improve the paper. The authors also thank A. Thompson, I. Shevchenko, N. Constantinou, M. Haigh and M. O'Donnell for their comments on the manuscript. I. Shevchenko also helped with the numerical simulations. The authors would also like to express their gratitude to the HPC team at Imperial College and A. Thomas for their help with computer clusters.

Appendix A. Tilted, drifting jets in a channel simulation

We ran a simulation in a channel configuration and imposed partial-slip boundary conditions on the meridional boundaries, which is given as

$$\frac{\partial u_i}{\partial y} + \frac{u_i}{\alpha} = 0, \tag{A 1}$$

where u_i is the zonal velocity in layer i, and $\alpha = 120$ km. Here, we used a 7200 km square domain having a grid resolution of 2048×2049, which is just to emphasise that jets tilt and drift irrespective of the domain size and grid resolution. Also, $\nu = 50$ m^2 s^{-1} and $\gamma = 10^{-8}$ s^{-1} were used to dissipate energy. The rest of the parameters were kept the same as given in § 2.1. The tilted, drifting jets are shown in figure 9. The tilt angle and drift speed are roughly 5° and 0.2 cm s^{-1}. The dynamics is more complex here, as accumulation of a positive/negative PV anomaly can be seen on the boundaries, which is caused by the drifting jets. A secondary circulation is then created along the boundaries, which transports PV. This way, PV of the system is conserved.

Appendix B. Dispersion relation in the two-layer QG model

The dispersion relation is derived by substituting $\psi_i = \widetilde{\psi}_i \mathrm{e}^{\mathrm{i}(kx+ly-\omega t)}$ in (2.1) and (2.2). The resulting linearised equations can be represented in the following matrix form:

$$\begin{bmatrix} \omega(k^2+l^2+S_1)+k(\beta-U_b(k^2+l^2)) & -S_1\omega + S_1U_bk \\ \quad +\mathrm{i}\nu(k^4+l^4) & \\ -S_2\omega & \omega(k^2+l^2+S_2) - lT_x + k(\beta - U_bS_2) \\ & \quad +\mathrm{i}\nu(k^4+l^4)+\mathrm{i}\gamma(l^2+l^2) \end{bmatrix} \begin{bmatrix} \widetilde{\psi}_1 \\ \widetilde{\psi}_2 \end{bmatrix} = 0. \tag{B 1}$$

For the existence of non-trivial solutions, the determinant of the matrix must vanish, which results in two frequency solutions for each wavenumber pair (k, l). The real parts of the frequencies predict two different drift velocities, which are in opposite directions and possess different magnitudes, corresponding to the wavenumber. For the purpose of comparing drift velocities, the frequency solution giving the same direction of drift as the jets in the simulations is considered. It turns out that the chosen frequency also predicts faster drift out of the two frequencies.

https://doi.org/10.1017/jfm.2018.260 Published online by Cambridge University Press

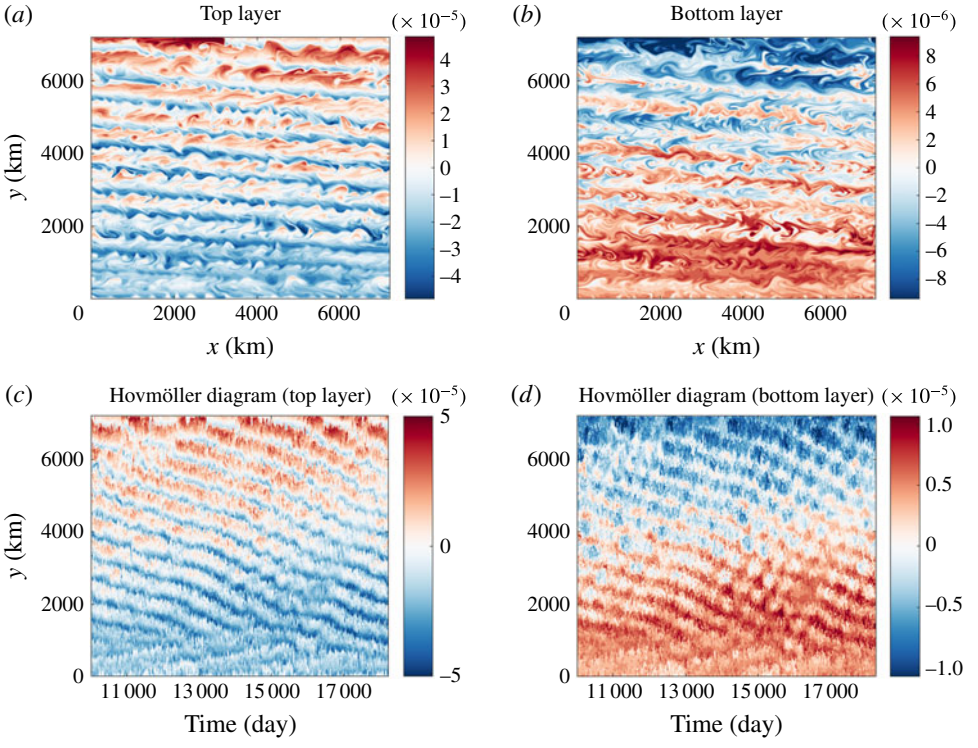


FIGURE 9. (Colour online) General flow patterns and equilibration of the jets in a channel. (*a*,*b*) Snapshots of the PV anomaly (colour bar units are in s^{-1}) field in the top layer ($\nabla^2\psi_1 + S_1(\psi_2 - \psi_1)$) and bottom layer ($\nabla^2\psi_2 + S_2(\psi_1 - \psi_2)$) for medium-slope configuration. (*c*,*d*) Hovmöller diagram of the PV anomaly field in the top and bottom layers (PV along a cross-section at the centre of the domain is plotted against time).

Appendix C. Derivation of the QG equations in a tilted, non-stationary frame of reference

From (3.1) and (3.2), the variables can be represented as a sum of the time-mean $(\overline{Q}_i,\ \overline{\psi}_i)$ and eddy components $(Q_i',\ \psi_i')$:

$$\begin{aligned}\left[\frac{\partial}{\partial t} - c\frac{\partial}{\partial q}\right](\overline{Q}_1 + Q_1') &= -\left(\frac{\partial(\overline{\psi}_1 + \psi_1')}{\partial p} - U_b\sin\theta\right)\left(\frac{\partial(\overline{Q}_1 + Q_1')}{\partial q} + (\beta + S_1U_b)\cos\theta\right)\\ &\quad + \left(\frac{\partial(\overline{\psi}_1 + \psi_1')}{\partial q} - U_b\cos\theta\right)\left(\frac{\partial(\overline{Q}_1 + Q_1')}{\partial p} + (\beta + S_1U_b)\sin\theta\right)\\ &\quad + \nu\nabla^4(\overline{\psi}_1 + \psi_1'),\end{aligned} \tag{C 1}$$

$$\begin{aligned}\left[\frac{\partial}{\partial t} - c\frac{\partial}{\partial q}\right](\overline{Q}_2 + Q_2') &= -\frac{\partial(\overline{\psi}_2 + \psi_2')}{\partial p}\left(\frac{\partial(\overline{Q}_2 + Q_2')}{\partial q} + (\beta - S_2U_b)\cos\theta - T_x\sin\theta\right)\\ &\quad + \frac{\partial(\overline{\psi}_2 + \psi_2')}{\partial q}\left(\frac{\partial(\overline{Q}_2 + Q_2')}{\partial p} + (\beta - S_2U_b)\sin\theta + T_x\cos\theta\right)\\ &\quad + \nu\nabla^4(\overline{\psi}_2 + \psi_2') - \gamma\nabla^2(\overline{\psi}_2 + \psi_2').\end{aligned} \tag{C 2}$$

https://doi.org/10.1017/jfm.2018.260 Published online by Cambridge University Press

The equations are then averaged over time to derive the time-mean equations. Note that $\overline{Q_i'} = \overline{\psi_i'} = 0$ and $\partial\overline{Q}_i/\partial p = \partial\overline{\psi}_i/\partial p = 0$ (the jets are purely zonal in the new configuration). Thus

$$\frac{\partial\overline{Q}_1}{\partial t} - c\frac{\partial\overline{Q}_1}{\partial q} = -\overline{\frac{\partial\psi_1'}{\partial p}\frac{\partial Q_1'}{\partial q}} + U_b\sin\theta\frac{\partial\overline{Q}_1}{\partial q} + \overline{\frac{\partial\psi_1'}{\partial q}\frac{\partial Q_1'}{\partial p}} + (\beta + S_1U_b)\sin\theta\frac{\partial\overline{\psi_1}}{\partial q} + \nu\nabla^4\overline{\psi}_1, \tag{C 3}$$

$$\frac{\partial\overline{Q}_2}{\partial t} - c\frac{\partial\overline{Q}_2}{\partial q} = -\overline{\frac{\partial\psi_2'}{\partial p}\frac{\partial Q_2'}{\partial q}} + \overline{\frac{\partial\psi_2'}{\partial q}\frac{\partial Q_2'}{\partial p}} + [(\beta - S_2U_b)\sin\theta + T_x\cos\theta]\frac{\partial\overline{\psi_2}}{\partial q} + \nu\nabla^4\overline{\psi}_2 - \gamma\nabla^2\overline{\psi}_2. \tag{C 4}$$

For clarity, we retain the time derivatives in the mean PV. In equilibrium, the time derivative terms vanish. We then replace the streamfunction by velocity ($\boldsymbol{u}_i = (u_i,\ v_i) = (-\partial\psi_i/\partial q,\ \partial\psi_i/\partial p)$), introduce relative vorticity ($\zeta_i = \nabla^2\psi_i$), and represent the nonlinear terms in the flux form (note that $\boldsymbol{\nabla}\cdot\boldsymbol{u}_i' = 0$ from the continuity equation). The final time-mean equations are given as

$$\frac{\partial\overline{Q}_1}{\partial t} = -\boldsymbol{\nabla}\cdot\overline{(\boldsymbol{u}_1'Q_1')} + (c + U_b\sin\theta)\frac{\partial\overline{Q}_1}{\partial q} - (\beta + S_1U_b)\sin\theta\ \overline{u}_1 + \nu\nabla^2\overline{\zeta}_1, \tag{C 5}$$

$$\frac{\partial\overline{Q}_2}{\partial t} = -\boldsymbol{\nabla}\cdot\overline{(\boldsymbol{u}_2'Q_2')} + c\frac{\partial\overline{Q}_2}{\partial q} - [(\beta - S_2U_b)\sin\theta + T_x\cos\theta]\,\overline{u}_2 + \nu\nabla^2\overline{\zeta}_2 - \gamma\overline{\zeta}_2. \tag{C 6}$$

REFERENCES

ABERNATHEY, R. & CESSI, P. 2014 Topographic enhancement of eddy efficiency in baroclinic equilibration. *J. Phys. Oceanogr.* **44** (8), 2107–2126.

ABERNATHEY, R., MARSHALL, J., MAZLOFF, M. & SHUCKBURGH, E. 2010 Enhancement of mesoscale eddy stirring at steering levels in the Southern Ocean. *J. Phys. Oceanogr.* **40** (1), 170–184.

ARBIC, B. K. & FLIERL, G. R. 2004 Effects of mean flow direction on energy, isotropy, and coherence of baroclinically unstable beta-plane geostrophic turbulence. *J. Phys. Oceanogr.* **34** (1), 77–93.

BALDWIN, M. P., RHINES, P. B., HUANG, H. P. & MCINTYRE, M. E. 2007 The jet-stream conundrum. *Science* **315** (5811), 467–468.

BARTHEL, A., HOGG, A., WATERMAN, S. & KEATING, S. 2017 Jet–topography interactions affect energy pathways to the deep Southern Ocean. *J. Phys. Oceanogr.* **47** (7), 1799–1816.

BEEBE, R. F., INGERSOLL, A. P., HUNT, G. E., MITCHELL, J. L. & MÜLLER, J. P. 1980 Measurements of wind vectors, eddy momentum transports, and energy conversions in Jupiter's atmosphere from Voyager 1 images. *Geophys. Res. Lett.* **7** (1), 1–4.

BERLOFF, P. 2005*a* On dynamically consistent eddy fluxes. *Dyn. Atmos. Oceans* **38** (3), 123–146.

BERLOFF, P. 2005*b* On rectification of randomly forced flows. *J. Mar. Res.* **63** (3), 497–527.

BERLOFF, P. & KAMENKOVICH, I. 2013*a* On spectral analysis of mesoscale eddies. Part I: linear analysis. *J. Phys. Oceanogr.* **43** (12), 2505–2527.

BERLOFF, P. & KAMENKOVICH, I. 2013*b* On spectral analysis of mesoscale eddies. Part II: nonlinear analysis. *J. Phys. Oceanogr.* **43** (12), 2528–2544.

https://doi.org/10.1017/jfm.2018.260 Published online by Cambridge University Press

BERLOFF, P., KAMENKOVICH, I. & PEDLOSKY, J. 2009*a* A mechanism of formation of multiple zonal jets in the oceans. *J. Fluid Mech.* **628**, 395–425.

BERLOFF, P., KAMENKOVICH, I. & PEDLOSKY, J. 2009*b* A model of multiple zonal jets in the oceans: dynamical and kinematical analysis. *J. Phys. Oceanogr.* **39** (11), 2711–2734.

BERLOFF, P., KARABASOV, S., FARRAR, J. T. & KAMENKOVICH, I. 2011 On latency of multiple zonal jets in the oceans. *J. Fluid Mech.* **686**, 534–567.

BOLAND, E., THOMPSON, A. F., SHUCKBURGH, E. & HAYNES, P. 2012 The formation of nonzonal jets over sloped topography. *J. Phys. Oceanogr.* **42** (10), 1635–1651.

BUCKINGHAM, C. E. & CORNILLON, P. C. 2013 The contribution of eddies to striations in absolute dynamic topography. *J. Geophys. Res. Oceans* **118** (1), 448–461.

CHAN, C. J., PLUMB, R. A. & CEROVECKI, I. 2007 Annular modes in a multiple migrating zonal jet regime. *J. Atmos. Sci.* **64** (11), 4053–4068.

CHARNEY, J. C. 1971 Geostrophic turbulence. *J. Atmos. Sci.* **28**, 1087–1095.

CHELTON, D. B., DESZOEKE, R. A., SCHLAX, M. G., EL NAGGAR, K. & SIWERTZ, N. 1998 Geographical variability of the first baroclinic Rossby radius of deformation. *J. Phys. Oceanogr.* **28** (3), 433–460.

CHEMKE, R. & KASPI, Y. 2015*a* The latitudinal dependence of atmospheric jet scales and macroturbulent energy cascades. *J. Atmos. Sci.* **72** (10), 3891–3907.

CHEMKE, R. & KASPI, Y. 2015*b* Poleward migration of eddy-driven jets. *J Adv. Model. Earth Syst.* **7** (3), 1457–1471.

CHEN, C. & KAMENKOVICH, I. 2013 Effects of topography on baroclinic instability. *J. Phys. Oceanogr.* **43** (4), 790–804.

CHEN, C., KAMENKOVICH, I. & BERLOFF, P. 2015 On the dynamics of flows induced by topographic ridges. *J. Phys. Oceanogr.* **45** (3), 927–940.

CHEN, C., KAMENKOVICH, I. & BERLOFF, P. 2016 Eddy trains and striations in quasigeostrophic simulations and the ocean. *J. Phys. Oceanogr.* **46** (9), 2807–2825.

CHO, J. Y. K. & POLVANI, L. M. 1996 The emergence of jets and vortices in freely evolving, shallow-water turbulence on a sphere. *Phys. Fluids* **8** (6), 1531–1552.

CONNAUGHTON, C. P., NADIGA, B. T., NAZARENKO, S. V. & QUINN, B. E. 2010 Modulational instability of Rossby and drift waves and generation of zonal jets. *J. Fluid Mech.* **654**, 207–231.

CONSTANTINOU, N. C., FARRELL, B. F. & IOANNOU, P. J. 2014 Emergence and equilibration of jets in beta-plane turbulence: applications of stochastic structural stability theory. *J. Atmos. Sci.* **71** (5), 1818–1842.

CRAVATTE, S., KESSLER, W. S. & MARIN, F. 2012 Intermediate zonal jets in the tropical Pacific Ocean observed by Argo floats. *J. Phys. Oceanogr.* **42** (9), 1475–1485.

CRAVATTE, S., KESTENARE, E., MARIN, F., DUTRIEUX, P. & FIRING, E. 2017 Subthermocline and intermediate zonal currents in the tropical Pacific Ocean: paths and vertical structure. *J. Phys. Oceanogr.* **47** (9), 2305–2324.

DRITSCHEL, D. G. & MCINTYRE, M. E. 2008 Multiple jets as PV staircases: the Phillips effect and the resilience of eddy-transport barriers. *J. Atmos. Sci.* **65** (3), 855–874.

DUNKERTON, T. J. & SCOTT, R. K. 2008 A barotropic model of the angular momentum-conserving potential vorticity staircase in spherical geometry. *J. Atmos. Sci.* **65** (4), 1105–1136.

FARRELL, B. F. & IOANNOU, P. J. 2007 Structure and spacing of jets in barotropic turbulence. *J. Atmos. Sci.* **64** (10), 3652–3665.

GIERASCH, P. J., CONRATH, B. J. & MAGALHA, J. A. 1986 Zonal mean properties of Jupiter's upper troposphere from Voyager infrared observations. *Icarus* **67** (3), 456–483.

HANNACHI, A., JOLLIFFE, I. T. & STEPHENSON, D. B. 2007 Empirical orthogonal functions and related techniques in atmospheric science: a review. *Intl J. Climatol.* **27** (9), 1119–1152.

HART, J. E. 1975 Baroclinic instability over a slope. Part I: linear theory. *J. Phys. Oceanogr.* **5** (4), 625–633.

HRISTOVA, H. G., PEDLOSKY, J. & SPALL, M. A. 2008 Radiating instability of a meridional boundary current. *J. Phys. Oceanogr.* **38** (10), 2294–2307.

HUANG, H. P. & ROBINSON, W. A. 1998 Two-dimensional turbulence and persistent zonal jets in a global barotropic model. *J. Atmos. Sci.* **55** (4), 611–632.

https://doi.org/10.1017/jfm.2018.260 Published online by Cambridge University Press

INGERSOLL, A. P., BEEBE, R. F., MITCHELL, J. L., GARNEAU, G. W., YAGI, G. M. & MÜLLER, J. P. 1981 Interaction of eddies and mean zonal flow on Jupiter as inferred from Voyager 1 and 2 images. *J. Geophys. Res. Space Phys.* **86** (A10), 8733–8743.

INGERSOLL, A. P., GIERASCH, P. J., BANFIELD, D., VASAVADA, A. R. & TEAM, G. I. 2000 Moist convection as an energy source for the large-scale motions in Jupiter's atmosphere. *Nature* **403** (6770), 630–632.

KAMENKOVICH, I., BERLOFF, P. & PEDLOSKY, J. 2009 Role of eddy forcing in the dynamics of multiple zonal jets in a model of the North Atlantic. *J. Phys. Oceanogr.* **39** (6), 1361–1379.

KARABASOV, S. A., BERLOFF, P. & GOLOVIZNIN, V. M. 2009 Cabaret in the ocean gyres. *Ocean Model.* **30** (2), 155–168.

KRAMER, W., VAN BUREN, M. G., CLERCX, H. J. H. & VAN HEIJST, G. J. F. 2006 β-plane turbulence in a basin with no-slip boundaries. *Phys. Fluids* **18** (2), 026603.

LU, J. & SPEER, K. 2010 Topography, jets, and eddy mixing in the Southern Ocean. *J. Mar. Res.* **68** (3–1), 479–502.

MALTRUD, M. E. & VALLIS, G. K. 1991 Energy spectra and coherent structures in forced two-dimensional and beta-plane turbulence. *J. Fluid Mech.* **228**, 321–342.

MARSTON, J. B., CONOVER, E. & SCHNEIDER, T. 2008 Statistics of an unstable barotropic jet from a cumulant expansion. *J. Atmos. Sci.* **65** (6), 1955–1966.

MAXIMENKO, N. A., BANG, B. & SASAKI, H. 2005 Observational evidence of alternating zonal jets in the world ocean. *Geophys. Res. Lett.* **32**, L12607.

MCINTYRE, M. E. 1982 How well do we understand the dynamics of stratospheric warmings? *J. Meteorol. Soc. Japan* II **60** (1), 37–65.

MELNICHENKO, O. V., MAXIMENKO, N. A., SCHNEIDER, N. & SASAKI, H. 2010 Quasi-stationary striations in basin-scale oceanic circulation: vorticity balance from observations and eddy-resolving model. *Ocean Dyn.* **60** (3), 653–666.

NADIGA, B. T. 2006 On zonal jets in oceans. *Geophys. Res. Lett.* **33**, L12607.

NAKANO, H. & HASUMI, H. 2005 A series of zonal jets embedded in the broad zonal flows in the Pacific obtained in eddy-permitting ocean general circulation models. *J. Phys. Oceanogr.* **35** (4), 474–488.

PANETTA, R. L. 1993 Zonal jets in wide baroclinically unstable regions: persistence and scale selection. *J. Atmos. Sci.* **50** (14), 2073–2106.

QIU, B., CHEN, S. & SASAKI, H. 2013 Generation of the North Equatorial Undercurrent jets by triad baroclinic Rossby wave interactions. *J. Phys. Oceanogr.* **43** (12), 2682–2698.

READ, P. L., CONRATH, B. J., FLETCHER, L. N., GIERASCH, P. J., SIMON-MILLER, A. A. & ZUCHOWSKI, L. C. 2009 Mapping potential vorticity dynamics on Saturn: zonal mean circulation from Cassini and Voyager data. *Planet. Space Sci.* **57** (14), 1682–1698.

RHINES, P. B. 1975 Waves and turbulence on a beta-plane. *J. Fluid Mech.* **69** (03), 417–443.

RICHARDS, K. J., MAXIMENKO, N. A., BRYAN, F. O. & SASAKI, H. 2006 Zonal jets in the Pacific Ocean. *Geophys. Res. Lett.* **33**, L03605.

SCOTT, R. K. & POLVANI, L. M. 2007 Forced-dissipative shallow-water turbulence on the sphere and the atmospheric circulation of the giant planets. *J. Atmos. Sci.* **64** (9), 3158–3176.

SINHA, B. & RICHARDS, K. J. 1999 Jet structure and scaling in Southern Ocean models. *J. Phys. Oceanogr.* **29** (6), 1143–1155.

SMITH, S. 2007 Eddy amplitudes in baroclinic turbulence driven by nonzonal mean flow: shear dispersion of potential vorticity. *J. Phys. Oceanogr.* **37** (4), 1037–1050.

SOKOLOV, S. & RINTOUL, S. R. 2007 Multiple jets of the Antarctic circumpolar current south of Australia. *J. Phys. Oceanogr.* **37** (5), 1394–1412.

SRINIVASAN, K. 2013 *Stochastically Forced Zonal Flows*. University of California.

SRINIVASAN, K. & YOUNG, W. R. 2012 Zonostrophic instability. *J. Atmos. Sci.* **69** (5), 1633–1656.

STERN, A., NADEAU, L. P. & HOLLAND, D. 2015 Instability and mixing of zonal jets along an idealized continental shelf break. *J. Phys. Oceanogr.* **45** (9), 2315–2338.

SUKORIANSKY, S., DIKOVSKAYA, N. & GALPERIN, B. 2007 On the arrest of inverse energy cascade and the Rhines scale. *J. Atmos. Sci.* **64** (9), 3312–3327.

https://doi.org/10.1017/jfm.2018.260 Published online by Cambridge University Press

THOMPSON, A. F. 2010 Jet formation and evolution in baroclinic turbulence with simple topography. *J. Phys. Oceanogr.* **40** (2), 257–278.

THOMPSON, A. F. & NAVEIRA GARABATO, A. C. 2014 Equilibration of the Antarctic circumpolar current by standing meanders. *J. Phys. Oceanogr.* **44** (7), 1811–1828.

THOMPSON, A. F. & RICHARDS, K. J. 2011 Low frequency variability of Southern Ocean jets. *J. Geophys. Res. Oceans* **116**, C09022.

THOMPSON, A. F. & YOUNG, W. R. 2007 Two-layer baroclinic eddy heat fluxes: zonal flows and energy balance. *J. Atmos. Sci.* **64** (9), 3214–3231.

TRÉGUIER, A. M. & PANETTA, R. L. 1994 Multiple zonal jets in a quasigeostrophic model of the Antarctic circumpolar current. *J. Phys. Oceanogr.* **24** (11), 2263–2277.

VALLIS, G. K. 2017 *Atmospheric and Oceanic Fluid Dynamics*. Cambridge University Press.

VALLIS, G. K. & MALTRUD, M. E. 1993 Generation of mean flows and jets on a beta plane and over topography. *J. Phys. Oceanogr.* **23** (7), 1346–1362.

VAN SEBILLE, E., KAMENKOVICH, I. & WILLIS, J. K. 2011 Quasi-zonal jets in 3-D Argo data of the Northeast Atlantic. *Geophys. Res. Lett.* **38**, L02606.

WANG, J., SPALL, M. A., FLIERL, G. R. & MALANOTTE-RIZZOLI, P. 2012 A new mechanism for the generation of quasi-zonal jets in the ocean. *Geophys. Res. Lett.* **39**, L10601.

WILLIAMS, G. P. 1979 Planetary circulations: 2. The Jovian quasi-geostrophic regime. *J. Atmos. Sci.* **36** (5), 932–969.

WILLIAMS, G. P. 2003 Jovian dynamics. Part III: multiple, migrating, and equatorial jets. *J. Atmos. Sci.* **60** (10), 1270–1296.

YOUNG, R. M. B. & READ, P. L. 2017 Forward and inverse kinetic energy cascades in Jupiter's turbulent weather layer. *Nat. Phys.* **13** (11), 1135.

YOUNGS, M. K., THOMPSON, A. F., LAZAR, A. & RICHARDS, K. 2017 ACC meanders, energy transfer, and mixed barotropic–baroclinic instability. *J. Phys. Oceanogr.* **47** (6), 1291–1305.

https://doi.org/10.1017/jfm.2018.260 Published online by Cambridge University Press